FDTD and Empirical Exploration of Human Body and UWB Radiation Interaction on TOF Ranging

Timothy Otim, Alfonso Bahillo, Luis E. Díez, Peio Lopez-Iturri, and Francisco Falcone

***Abstract*—In time of flight (TOF) based human ranging systems, target sensors are often mounted on or close to the human body which may raise non-line-of-sight (NLOS) cases and lead to significant ranging errors depending on the relative position between the body, Transmitter (Tx) and Receiver (Rx). In recent years, Ultrawideband (UWB) has become a very popular technology for human TOF ranging but its human body interactions have not been studied yet extensively. In this letter, the UWB and human body interaction is explored by the Finite Difference Time Domain (FDTD) technique, and the obtained E-field strength variation results are validated by means of commercially available UWB kits. Additionally, an UWB ranging error model with respect to the human body shadowing effect is proposed and evaluated by extensive measurements i.e., in indoor environments, LOS and NLOS are found to be well modelled by a Gaussian and Gamma distributions, respectively while in outdoor fields, LOS and NLOS are both modelled by Gaussian distributions. The main conclusion of this work is that there is a clear pattern between a gain in the E-field strength and TOF ranging errors. It can be established that in a worst-case scenario, a gain of 4–18 dB is observed which corresponds to about 30–60 cm of TOF ranging errors.**

***Index Terms*—FDTD, human body, UWB, TOF, Ranging**

I. Introduction

UNDENIABLY, Ultrawideband (UWB) technology has gained a lot of interest in the academic and industry research thanks to properties such as high bandwidth, ability to have extremely accurate location estimates, immunity to fading, low power transmission and low-cost implementation [1] . A key application and one of the most relevant nowadays of UWB systems is in localization and navigation systems. The huge bandwidth available of 500 MHz or more allows UWB technology to offer TOF based ranging measurements with centimeter accuracies even in severe multipath environments [2]. However, in NLOS situations, the aforementioned performance deteriorates dramatically, including when the user's body blocks the line-of-sight (LOS) path between the Tx and the Rx. Investigations of human body effects on UWB have somewhat been covered in the literature especially in [3], but most of the works present antenna design and channel characterization of off-body, on-body, and in-body propagation channels using path loss or time delay statistics [3]–[5], leaving aside the applicability of such studies in body area network applications. To the best of our knowledge, no work has been found in the literature that explores the relationship between UWB TOF ranging and a gain in the E–field strength.

Therefore, the specific contribution of this letter is three-fold: a) to provide a preliminary analysis of the interaction between UWB pulses and the human body by means of FDTD and empirically using commercially available UWB kits, b) to explicitly explore the relationship between a gain in the E–field strength and TOF ranging errors in realistic indoor and outdoor environments for a male and female subject, and c) to propose and evaluate UWB ranging error models which consider the human body shadowing effect.

II. FDTD Simulation Procedure

Studies of the human body effect on E-fields require electromagnetic computation for a better understanding of the distribution of fields around the body. In this work, the method of numerical analysis has been performed using an in-house developed FDTD model, since it is the most used technique when analysis of a digital anatomical model of a human body is to be considered. In [6]–[8], a more detailed description of the FDTD is done, however this letter follows the methods provided in [9] to simulate the UWB and human body interaction at UWB 3900 MHz. In the simulations, the sampling nodes were properly taken to ensure that a suitable representation of the human body is made and to achieve this requirement, the grid computation cell was set to dimensions of 2 mm $\times$ 2 mm $\times$ 2 mm. The tissues in each node were allocated a permittivity and conductivity according to the frequency of 3900 MHz [10]. A 3D human body with a 2 mm resolution from the Visible Human Project sponsored by the National Library of Medicine in the USA is used for simulation purposes [11]. This model is based on anatomical slices from a male cadaver, aged 38, 1.80 m height and a mass of 90 kg.

In this letter, only the illumination plane is considered as the main RF contributor which can impinge on the human body at different azimuths ϕ. The test angles are given by : 0° and 45° referring to LOS, 90° which is quasi-LOS (QLOS) since part of human body is located between the Tx and Rx, and 135°, 180 ° – both considered as NLOS as the whole body is completely blocking the direct LOS between the Tx and Rx. The relation between ϕ and the case scenario (S) is reported in [12] as :

$$S = \begin{cases} LOS, & \phi \in [0°, 67.5°] \\ QLOS, & \phi \in (67.5°, 112.5°) \\ NLOS, & \phi \in [112.5°, 180°] \end{cases} \quad (1)$$

T. Otim, A. Bahillo, L. E. Díez are with the Faculty of Engineering, University of Deusto, Av. Universidades, 24, 48007, Bilbao, Spain, e-mail: {otim.timothy, alfonso.bahillo, luis.enrique.diez}@deusto.es.

P. Lopez-Iturri, F. Falcone are with the Department of Electric, Electronic and Communication Engineering and with the Institute for Smart Cities, Public University of Navarra, 31006, Pamplona, Spain, e-mail: {peio.lopez, francisco.falcone}@unavarra.es.

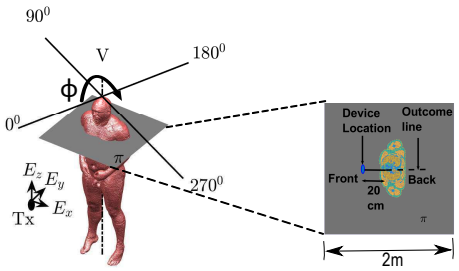

Fig. 1: 3D computational volume of the human body, where V is the rotational axis, π is the outcome plane. The outcome plane is a cross section of the anatomical body at approximately 2/3 of the body height.

Instead of modifying the wavefront phase which illuminates the human body model, the angles are obtained by rotating the human body along the vertical axis *V* as seen in Fig. 1, and we keep Y =0 plane as the illuminated plane in all the simulations. Inside the computational domain, only the human body is considered as the main obstacle to the signal path between the Tx and the Rx, which is located in the hands – 20 cm from the chest since this is a usual place for texting or looking at the screen of a smart phone when locating your position in a real world scenario.

A. Simulation Results

By normalizing the E-field strength in presence of the human body E_b with respect to the incident wave power E_r, (2) is used to assess the E-field strength variation across the angles ϕ and distances (d) between the Tx and Rx.

$$\Delta \textit{E-field strength}(d,\phi)_{[dB]} = 20\log_{10}(E_b/E_r) \quad (2)$$

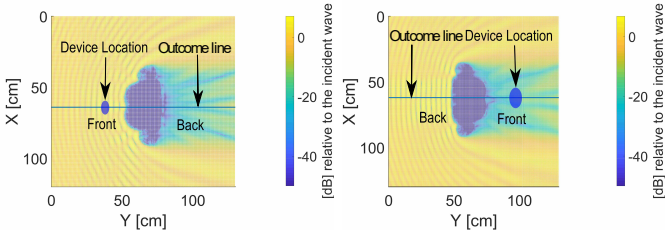

(a) (b)

Fig. 2: Spatial variability of the E-field through plane π, where ϕ is at: (a) 0° and (b) 180°. The Y [cm] and X [cm] are dimensions along the outcome plane

Looking at Fig. 3, it is quite clear that the orientation of the user has a direct influence on the obtained RSS values. On one hand exists NLOS (135° and 180°) in which there is a clearly power attenuation, and on the other hand LOS/QLOS (0°, 45°, 90°) in which there are small power variations due to the peaks/valleys of the stationary wave.This effect is further demonstrated in Fig. 2 for the extreme LOS and NLOS cases. Since the human who is holding the Rx is facing the Tx antenna in Fig. 2a, the human body has very little

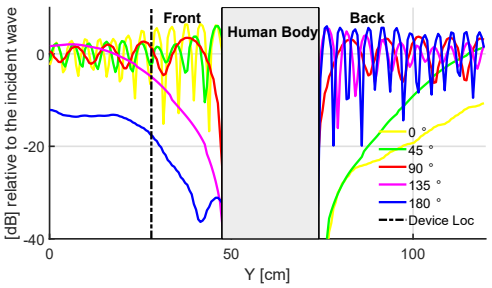

Fig. 3: Simulated results representing the E-field strength variations through the outcome line.

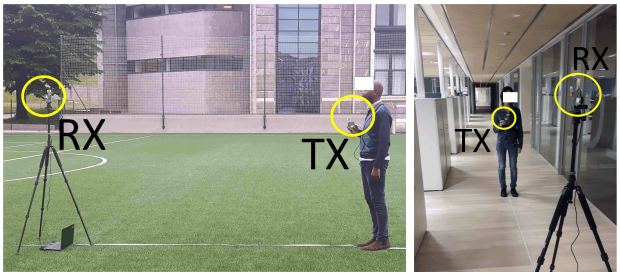

(a) (b)

Fig. 4: Measurement setup whereby (a) Subject B1 in an outdoor field, and (b) Subject B2 in an indoor environment.

effect on the received E-field strength however in Fig. 2b the Rx is obstructed completely by the human body, and hence lies in the maximum shadowing zone. A comparison of the simulation and measurement results is made in Fig. 5.

III. Measurements Description

Experiments were set up firstly with the aim of validating the simulation results obtained in the previous section, and secondly exploring the impact of UWB and human body interaction on TOF ranging. Regarding UWB, the E-field strength measurements were performed with several TREK1000 development kits manufactured by Decawave and an omnidirectional UWB Partron dielectric chip antenna manufactured by Abracon [13]. According to [2], TREK1000 development kits are the best UWB commercial products for ranging. The nodes are fully compliant with the IEEE 802.15.4-2011 UWB standard and make it possible to achieve ranging measurements using two-way ranging measurements. For the purpose of this measurement campaign, we modified the software provided by the manufacturer. In this way, we were able to simultaneously estimate the RSS and TOF between a pair of UWB nodes at a rate of 3.5 Hz. For longer ranges, the nodes were configured to work with a 110 kb/s data rate and in the channel 2 (3990 MHz), which we considered to be equivalent to 3900 MHz. Firstly, the experiments were carried out at the outdoor field at the University of Deusto in Spain–(see Fig. 4a), with 69 m long, and 41 m wide dimensions.

The experiments were again repeated along the main corridor of DeustoTech offices within the Faculty of Engineering at the same University with dimensions: 13 m wide, 83 m long,

and 2.5 m high – (see Fig. 4b). A first measurement campaign was carried out to obtain the RSS and TOF estimate without the influence of the body as a reference for further comparisons. In a second campaign, two subjects were considered for the measurements. Similar to the simulations, the first subject (B1) was a male 1.73 m height and 77 kg mass. The second subject (B2) was a female of 1.66 m height and 50 kg mass. Due to UWB sensor's poor sensitivity at 180 ° (difficulty in receiving packets), six distances between the body and the Rx were investigated, from 1 to 6 m, with a 1-m step, which (range) is in unison with [12]. Similar to simulations, the Tx was held by the subjects at chest level. In both environments, the Rx was mounted on a mast 1.68 m high and placed at a fixed vertical and horizontal position. The Tx was mounted on a mast 1.56 m high, and was moved along a straight line with a 1m step. The small difference in height is due to the use of different tripod models. A laptop was connected to the Rx to store all measurements, and preliminary calculations were done using MATLAB software. At a rate of 3.5 Hz, measurements were recorded over a period of 30 s, generating at-least 100 sets of simultaneous RSS and TOF estimations for each distance and rotation.

A. Measurement Results

The estimate of the receive power level (in dBm) is performed using the Channel Impulse Response Power, Pulse repetition frequency constant, Preamble Accumulation Count value, accessed from the TREK1000 register [13]. To validate the FDTD simulation results, the expression in (2) is again used to properly work out the effect of human body and UWB interaction on the RSS. And so, the parameters used in calculation include, RSS obtained in the absence and presence of the human body for each body orientation and the distance – for the outdoor propagation environment.

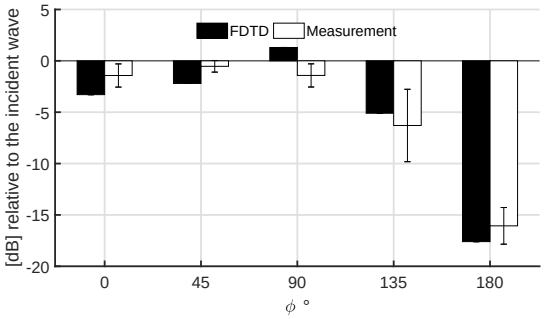

Fig. 5: Comparison of FDTD and measurement results for the male subject in an outdoor/ free space environment. The error bars are the standard deviations (SD).

In Fig. 5, the bars are averaged over six sets of measurements from six positions. A relatively good agreement is seen between the measurement and simulation results, which validates the numerical simulation.

Noticeably, in LOS or QLOS, a power gain of 0–2 dB for measurement and 1–3 dB in simulation is observed if the Rx moves slightly closer/further from the body. In contrast with NLOS, gains of 5–18 dB for simulations and 6–17 dB in measurements are seen because when the plane wave approaches the human body with the back facing the Tx, as much of the power gets absorbed by the body due to the dielectric losses in the human body – see (Fig. 2b), and the wave reaches the Rx through creeping wave propagation [14].

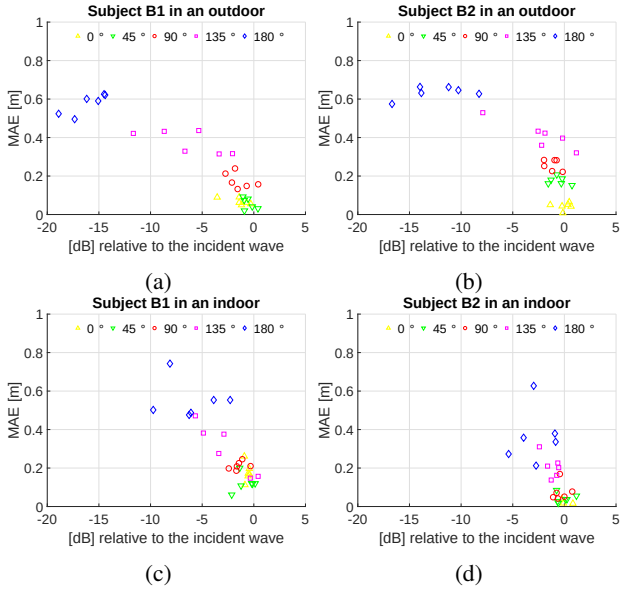

Fig. 6: Effect of the E–field strength variation on TOF ranging.

IV. Ranging

The range between the Tx and Rx is determined when the TOF and the speed of propagation of radio waves are known. And so, the TOF ranging error ϵ_ϕ is defined as the difference between estimated range $\hat{d}$ and the actual range d.

A. Effect of E–field strength variations

In the following section, we explore the effect of E–field strength variations on the ranging result. For each distance, at-least 600 TOF and RSS estimations are used in the calculation. For subjects B1 and B2, Fig. 6 shows how a gain in the E–field strength influences the calculated ranging mean absolute error (MAE) in different environments.

The first observation is existence of a clear relationship between the ranging error and a power gain due to having a Rx or Tx on or closer to the body. The results show that the error is generally increasing with a power gain due to the body. Similar to [15], in Fig. 6, we observe that the value of mean and variance of each test case varies a lot and a clear distinction exists between LOS, QLOS on one side, and NLOS on the other side. Under LOS, we observe relatively low power gains of 0–2dB which limit the ranging error to less than 20 cm, while with QLOS with gains of 0–4 dB, the mean error raises up to 30 cm. However, we observe significant power gains of 4–18 dB under NLOS, hence the mean error raising up to 60 cm.

B. Ranging Error Model

The histogram distribution of ranging errors for the extreme LOS (0°) and NLOS (180°) cases in the office and outdoor

field are showed in Fig. 7. As reported in [2], for indoor environments a Gaussian distribution is observed for LOS - (see Fig. 7a) and Gamma distribution for NLOS cases - (see Fig. 7b).

On the contrary, in the outdoor field, a Gaussian distribution is observed for both the LOS - (see Fig. 7c) and NLOS cases - (see Fig. 7d). With LOS scenarios, ϕ has a little effect on the ranging error as the mean error less than 20 cm is quite similar to the mean error obtained without the presence of the human body, however in NLOS, the effect of ϕ is very evident as expected. The long tail observed in Fig. 7b is because of the presence of severe multipath in indoor environments, while the behaviour of the distribution in Fig. 7d is due to wave propagation by the creeping wave phenomena.

In proposing a TOF ranging error model in (3), we took advantage of the clear distinction that exists between LOS,QLOS on the one hand and NLOS on the other hand observed in Fig. 6. In (3), the ranging error ϵ_ϕ is split the into LOS error ϵ_{LOS} (combining the LOS and QLOS cases) and the undetectable direct path (UDP) error ϵ_{UDP} brought about by NLOS human body shadowing [15].

$$\epsilon_\phi = \epsilon_{LOS} + \delta(P(\phi) - 1) \times \epsilon_{UDP} \tag{3}$$

The unit impulse function is given by

$$\delta(P(\phi) - 1) = \begin{cases} 0, & \phi \in [0°, 112.5°) \\ 1, & \phi \in [112.5°, 180°] \end{cases} \tag{4}$$

According to [15], the relationship between ϵ_{LOS}, ϵ_{NLOS} and ϵ_{UDP} is defined as

$$\epsilon_{UDP} = \epsilon_{NLOS} - \epsilon_{LOS} \tag{5}$$

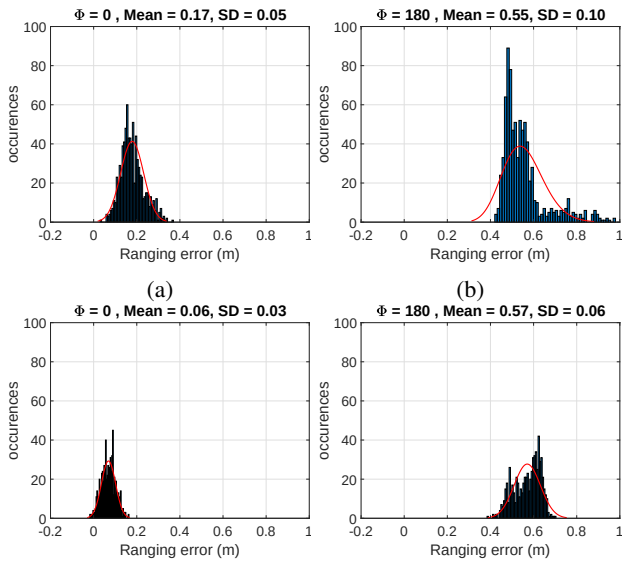

Fig. 7: TOF ranging error distribution for subject B1 in the office room for (a) and (b), and outdoor field for (c) and (d).

Based on the measurement data, the ranging error model proposed for the indoor environment is defined by the PDF in (6), which combines a Gaussian and Gamma distribution with a long tail on the positive error side for the LOS and NLOS cases, respectively.

$$f(\epsilon) = \frac{1}{\sigma\sqrt{2\pi}} e^{-\frac{(\epsilon-\mu_{LOS})^2}{2\sigma_{LOS}^2}} + \delta(P(\phi) - 1).\left(\lambda.e^{-\lambda\epsilon}.\frac{(\lambda\epsilon)^{k-1}}{\Gamma(k)} + c\right) \tag{6}$$

To work out the parameters for the proposed model, the combined ranging error distribution from both subjects B1 and B2 are utilized. Similar to the work in [16], the mean μ_{LOS} of the Gaussian distribution is obtained by examining the linear relationship between the MAE and the angles observed in Fig. 6. Using linear regression the relation between μ_{LOS} and ϕ is defined as

$$\mu_{LOS} = 0.03.\,\phi + 0.08. \tag{7}$$

Since this study involved 6 distances between the Tx and Rx, the MAE values were averaged to obtain a single point for the regression. Additionally, σ_{LOS} is set to 0.04 by averaging all the SD values of the combined LOS distributions. The parameters in Gamma distribution are obtained by fitting the combined NLOS histogram with λ = 11.15 and k = 0.02 and according to [2] and [16], the constant term c is equal to a 3% of the model's peak to cater for the uncertainty in the measurements.

In the outdoor scenario, basing on the measurement data, Gaussian assumptions are used to model range error distribution for LOS and NLOS cases as defined in (8)

$$f(\epsilon) = \frac{1}{\sigma\sqrt{2\pi}} e^{-\frac{(\epsilon-\mu_{LOS})^2}{2\sigma_{LOS}^2}} + \delta(P(\phi) - 1).\left(\frac{1}{\sigma\sqrt{2\pi}} e^{-\frac{(\epsilon-\mu_{UDP})^2}{2\sigma_{UDP}^2}}\right) \tag{8}$$

Similar to the previous indoor LOS scenario model, the relationship between μ_{LOS}, μ_{UDP} and ϕ for the respective cases is obtained by linear regression as

$$\mu_{LOS} = 0.10.\,\phi + 0.04. \tag{9}$$

$$\mu_{UDP} = 0.25.\,\phi - 0.32. \tag{10}$$

The σ in (8) is set to 0.02 and 0.10 for LOS and UDP respectively.

V. Conclusion

In this letter, a preliminary exploration of UWB and human body interaction is presented by FDTD and empirical techniques. Gains of 4–18 dB in the E-field strength are found in a worst case NLOS scenario, which explicitly correspond to ranging errors of 30–60 cm. It can be noted that human body shadowing is the main basis for NLOS in tracking of humans, which is the main motivation for this letter.

REFERENCES

[1] A. F. Molisch, "Ultra-Wide-Band Propagation Channels," *Proceedings of the IEEE*, vol. 97, no. 2, pp. 353–371, Feb. 2009.
[2] A. R. Jimenez Ruiz and F. Seco Granja, "Comparing Ubisense, BeSpoon, and DecaWave UWB Location Systems: Indoor Performance Analysis," *IEEE Transactions on Instrumentation and Measurement*, vol. 66, no. 8, pp. 2106–2117, Aug. 2017.
[3] P. Hall and Y. Hao, "Antennas and Propagation for Body-Centric Wireless Communications—Second Edition," *Wireless Communications*, pp. 1–375, 2012.
[4] M. Klemm, I. Kovcs, G. Pedersen, and G. Troster, "Novel small-size directional antenna for UWB WBAN/WPAN applications," *IEEE Transactions on Antennas and Propagation*, vol. 53, no. 12, pp. 3884–3896, Dec. 2005.
[5] R.-G. Garcia-Serna, C. Garcia-Pardo, and J.-M. Molina-Garcia-Pardo, "Effect of the Receiver Attachment Position on Ultrawideband Off-Body Channels," *IEEE Antennas and Wireless Propagation Letters*, vol. 14, pp. 1101–1104, 2015.
[6] M. Rycroft, "Computational electrodynamics, the finite-difference time-domain method," *Journal of Atmospheric and Terrestrial Physics*, vol. 58, no. 15, pp. 1817–1818, Nov. 1996.
[7] K. S. Kunz and R. J. Luebbers, *The Finite Difference Time Domain Method for Electromagnetics*. Boca Raton, FL CRC Press 1993.
[8] D. M. Sullivan, *Electromagnetic simulation using the FDTD method*. New York: Wiley-IEEE Press 2008.
[9] A. Bahillo, J. Blas, P. Fernández, R. M. Lorenzo, S. Mazuelas, and E. J. Abril, "E-field assessment errors associated with RF dosemeters for different angles of arrival," *Radiation protection dosimetry*, vol. 132, no. 1, pp. 51–56, 2008.
[10] "D.Andreuccetti, R.Fossi and C.Petrucci: An Internet resource for the calculation of the dielectric properties of body tissues in the frequency range 10 Hz - 100 GHz. IFAC-CNR, Florence (Italy), 1997," http://niremf.ifac.cnr.it/tissprop/, accessed: 2018-01-25.
[11] V. Spitzer, M. Ackerman, A. Scherzinger, and D. Whitlock, "The visible human male: A technical report," *Journal of the American Medical Informatics Association*, vol. 2, pp. 118–130, 1996.
[12] S. J. Ambroziak, L. M. Correia, R. J. Katulski, M. Mackowiak, C. Oliveira, J. Sadowski, and K. Turbic, "An Off-Body Channel Model for Body Area Networks in Indoor Environments," *IEEE Transactions on Antennas and Propagation*, vol. 64, no. 9, pp. 4022–4035, Sep. 2016.
[13] A. EVK, "TREK1000 Expansion Options Instructions," p. 12, 2016.
[14] D. Bresnahan and Y. Li, "Investigation of Creeping Wave Propagation Around the Human Head at ISM Frequencies," *IEEE Antennas and Wireless Propagation Letters*, vol. 16, pp. 2767–2770, 2017.
[15] Y. Gengt, "Modeling the effect of human body on TOA ranging for indoor human tracking with wrist mounted sensor," *16th International Symposium on Wireless Personal Multimedia Communications (WPMC), Atlantic City, NJ,*, pp. 1–6, 2013.
[16] Q. Tian, K. I.-K. Wang, and Z. Salcic, "Human Body Shadowing Effect on UWB-Based Ranging System for Pedestrian Tracking," *IEEE Transactions on Instrumentation and Measurement*, pp. 1–10, 2018.